Sains Malaysiana 50(1)(2021): 135-149
http://dx.doi.org/10.17576/jsm-2021-5001-14

Preparation and Characterization of Copper, Iron, and Nickel Doped Titanium Dioxide Photocatalysts for Decolorization of Methylene Blue

(Penyediaan dan Pencirian Fotomangkin daripada Tembaga, Besi dan Nikel Titanium Dioksida untuk Penyahwarnaan Metilena Biru)

JAWED QADERI, CHE ROZID MAMAT & AISHAH ABDUL JALIL

ABSTRACT

The visible-light response is a necessary condition for titanium dioxide (TiO_2) photocatalyst to function as a visible light active photocatalyst. This condition can be solved by investigation of the bandgaps and the optimization of doping levels of multivalency metal-doped TiO_2. In this study, pure and Cu, Fe, and Ni-doped TiO_2 photocatalysts were prepared by the sol-gel method. The photocatalysts were characterized using XRD, FTIR, FESEM, EDX, N_2 physisorption, and UV-Vis spectrophotometry techniques. The XRD patterns of all pure TiO_2 and Cu/TiO_2, Fe/TiO_2, and Ni/TiO_2 samples showed the dominant structure of the anatase TiO_2 phase. The presence of functional groups at the interface of TiO_2 particles was showed by FTIR. The FESEM analysis showed that the particle size of the prepared samples was uniform with spherical morphology. EDX results showed that TiO_2 has successfully incorporated Cu, Fe, and Ni metals onto its surface. The BET analysis showed that the specific surface area of the doped samples increased with the amount of doping. The optical properties of all samples were carried out using UV-DRS measurements and their obtained bandgap energies were in the range of 3.22 - 3.42 eV. The pure TiO_2 displayed more than 98% and 97% decolorization rates for MB solution at the end of irradiation time of 5 h under UV and visible light, respectively. Among the doped samples, 3 mol% Ni/TiO_2 and Cu/TiO_2 demonstrated the highest photocatalytic activity (97.65%) under UV light and 6 mol% Ni/TiO_2 under visible light for MB (96.86%) decolorization.

Keywords: Cu/TiO_2; Fe/TiO_2; Ni/TiO_2; photocatalyst; sol-gel; titanium dioxide (TiO_2)

ABSTRAK

Tindak balas cahaya nampak adalah syarat penting fotomangkin titanium dioksida (TiO_2) berfungsi sebagai fotomangkin cahaya tampak aktif. Keadaan ini boleh diselesaikan dengan penyelidikan jurang jalur dan pengoptimuman kandungan dopan logam pelbagai valensi dalam TiO_2. Dalam kajian ini, fotomangkin TiO_2 tulen dan yang didopkan dengan logam peralihan pada kala keempat iaitu, Cu, Fe, dan Ni, telah disediakan melalui kaedah sol-gel. Fotomangkin dicirikan menggunakan teknik XRD, FTIR, FESEM, EDX, N_2 dan spektrofotometri UV-Vis. Spektrum XRD bagi semua TiO_2 tulen dan Cu/TiO_2, Fe/TiO_2 dan Ni/TiO_2 menunjukkan struktur dominan fasa anatase TiO_2. Kehadiran ikatan kimia yang kuat antara permukaan zarah TiO_2 telah dibuktikan oleh FTIR. Analisis FESEM mendedahkan bahawa saiz zarah sampel yang disediakan seragam dengan morfologi sfera. Keputusan EDX menunjukkan TiO_2 telah berjaya didopkan dengan logam Cu, Fe dan Ni di atas permukaannya. Analisis BET menunjukkan kawasan permukaan khusus sampel dopan meningkat dengan jumlah bahan dopan. Sifat optik kesemua sampel telah diuji menggunakan kaedah pengukuran UV-DRS dan tenaga jalur yang diperoleh berada dalam julat 3.22 - 3.42 eV. Fotomangkin TiO_2 tulen menunjukkan lebih daripada 98% dan 97% kadar penguraian foto untuk MB pada penghujung masa penyinaran selama 5 jam di bawah sinaran UV dan cahaya nampak. Antara semua sampel TiO_2 yang berdop, 3 mol% Ni/TiO_2 dan Cu/TiO_2 menunjukkan aktiviti fotomangkin tertinggi (97.65%) di bawah cahaya UV dan 6 mol% Ni/TiO_2 di bawah cahaya tampak untuk MB (96.86%).

Kata kunci: Cu/TiO_2; Fe/TiO_2; Ni/TiO_2; fotomangkin; sol-gel; titanium dioksida (TiO_2)

INTRODUCTION

In the last decade, photocatalysis using light irradiation, a safe and desirable technique, has attracted considerable considerations as it is carried out at low temperature, normal pressure, and without the need for high input energy (Shehzad et al. 2018). Because of its attractive

properties, TiO_2 is a widely used photocatalyst among all metal oxide semiconductors. Such properties include availability and affordability, strong charge transfer efficiency, protection and corrosion resistance, powerful oxidation properties, and easy tuning (Adekoya et. 2019). While TiO_2 has several unique properties, its practical application is limited due to its high recombination charge rate, low quantum yield, and high bandgap energy (3.20 eV for anatase) (Edelmannová et al. 2018); so TiO_2 has only UV light activity (wavelength of less than 380 nm). It means that in this region of the spectrum, TiO_2 is mostly inactive under visible light, which is the largest part of the solar spectrum (Adekoya et al. 2019). Doping with small amounts of transition metals is the best way to improve the photocatalytic performance among the various modifications of TiO_2 usually applied. The advantages of metal doping include a decrease in the frequency of electron-hole pairs of recombination because of trapping of electrons by metal ions and an increase in the wavelength response to the visible region (Ali et al. 2017).

Nowadays, huge amounts of artificial and organic dyes are manufactured and consumed every day for coloring purposes in different sectors worldwide. Trace dye levels in effluent streams pose a significant threat to plants, livestock, atmosphere, and human health because of their poisonous and non-biodegradable existence (Kerkez-Kuyumcu et al. 2015). Among all the dyes, methylene blue (MB) which is a cationic dye, has been widely employed for dyeing cotton, wool, and silk. The risk of this dye being present in wastewater can arise from the effect of the burns to the eye, nausea, vomiting, and diarrhea (Salehi et al. 2012). Elimination of this dye from wastewater is regarded as a major environmental issue. Several methods have been suggested including biodegradation, coagulation, adsorption, and removal of membranes for the extraction of dye from wastewater (Ahmad & Puasa 2007; Derudi et al. 2007; Mo et al. 2008). The traditional techniques used are not damaging as a whole, they just convert water pollution from one phase to another. Heterogeneous photocatalysis has become a successful and environmental friendly alternative for the degradation of toxic organic dye materials, as this method decomposes dyes and colorants into harmless carbon dioxide and water molecules (Rauf & Ashraf 2009; Soutsas et al. 2010).

The main goal of this study was to prepare and improve a range of simple, stable, and efficient pure and doped TiO_2 photocatalysts with three different transition metals of the fourth period namely, copper (Cu), iron (Fe), and nickel (Ni) by the sol-gel method. Among various elements doped so far into TiO_2, Cu, Fe, and Ni have been widely studied and considered to be important owing to the narrow bandgap energies and their high light absorption capacities. The Cu, Fe, and Ni doping have been found to replace certain Ti^{4+} ions in substitutional sites of TiO_2, and to cause the segregation and incorporation of Cu, Fe, and Ni on the surface of, and into the interstitial sites of TiO_2. The concentration of each metal dopants was predetermined to be 3, 6, and 9 mol%. Despite a large number of studies have been carried out on these Cu, Fe, and Ni-doped TiO_2 systems, many aspects with regard to the role of elements species with multivalent states including Cu^{2+}, Fe^{3+}, and Ni^{2+} in the photocatalytic reaction remain unclear. The effects of adding three successive transition metal elements, Cu, Fe, and Ni as dopants were studied to enhance the TiO_2 photoresponse to the visible light spectrum and to increase the photocatalytic performance of the host semiconductor photocatalyst and the effects of the surface species on the photocatalytic activity were investigated by means of X-ray diffraction (XRD), Fourier transform infrared (FTIR), nitrogen physiosorption, Field Emission Scanning Electron Microscope (FESEM), Energy Dispersive X-ray (EDX) and diffuse reflectance spectra UV-Vis (DRS) spectroscopy. MB from the thiazine group of dyes was taken as the target pollutant to examine the effect of the structure of the dye on the photocatalytic decolorization process and to assess the photocatalytic efficiency of the photocatalysts under UV-Vis light irradiation.

Materials and Methods

Preparation of the photocatalysts

The preparation of Cu, Fe, and Ni-doped TiO_2 photocatalysts with different concentrations of Cu, Fe, and Ni (3, 6, and 9 mol%) was carried out using the sol-gel technique adopted from Rajamannan et al. (2014b) using titanium tetraisopropoxide (TTIP, purity 97%, Aldrich). The precursors for Cu, Fe, and Ni metals were $Cu(CH_3COO)_2$ (purity 98%, GCE), $FeCl_3$ anhydrous (purity 98%, GCE), and $Ni(NO_3)_2{\cdot}6H_2O$ (purity 96%, GCE), respectively, and isopropanol and water were used as the solvents for the precursors. For the synthesis of Cu, Fe, and Ni-doped TiO_2 samples, 90 mL of isopropanol and the exact quantities of $Cu(CH_3COO)_2$, $FeCl_3$, and $Ni(NO_3)_2{\cdot}6H_2O$ were dissolved in 10 mL of distilled water, respectively. The entire mixture of isopropanol and metals precursors dissolved in distilled water was continuously stirred at room temperature to obtain a homogenous solution and 10 mL of TTIP was added dropwise to the above mixture with mechanical stirring. The whole mixture of TTIP and isopropanol was continuously stirred using a magnetic stirrer for 5 h. The stirred solution was filtered using Whatman filter paper and washed several times using deionized water to remove the impurities. The precipitates were dried at 80 ºC for 5 h to evaporate the organic residues and other impurities. In order to obtain the desired anatase phase of pure TiO_2, the dried

powders were calcined at 500 ºC for 2 h. Finally, the calcined powders of Cu, Fe, and Ni-doped TiO_2 samples were grinded in an agate mortar to avoid agglomeration. In turn, pure TiO_2 reference was synthesised using the same procedure without the addition of metal precursors in order to compare the results obtained.

CHARACTERIZATION

Various analytical characterization techniques were used to determine the physicochemical properties such as structure, crystalline phase, composition, distribution of elements within the material, organic and inorganic bands of functional groups, morphology and elemental composition, surface area, absorption region of each photocatalyst in the spectrum and the bandgap energy, and the percentage decolorization, respectively. In all cases, sample of pure TiO_2 were also measured for blank comparison with the results obtained.

The identification for crystallinity of the photocatalysts was determined using Radaku SmartLab X-ray diffractometer (XRD) equipped with CuKα (λ = 0.15406 nm) radiation operating at 40 kV with 30 mA. The analysis was recorded in the range 2θ = 20 - 80° at room temperature with the increment 2° min^{-1}. The Fourier transform infrared (FTIR) spectra were recorded using PerkinElmer Spectrometer with resolution of 8 cm^{-1} in the range of 4000 - 400 cm^{-1} at KBr phase. BET surface area was measured by nitrogen physisorption at 77 K using NOVA touch 4LX (Quantachrome Instruments, USA) apparatus. Prior to analysis, the photocatalysts were outgassed under vacuum at ambient temperature for 12 h. The surface morphology and elemental composition of the samples were investigated by field emission scanning electron microscope (FESEM) CROSSBEAM 340 ZEISS with GEMINI column and energy dispersive X-ray analysis using OXFORD INSTRUMENTS X-Max^N system. The diffuse reflectance spectra UV-Vis (DRS) was performed at room temperature using UV-3600 Plus Shimadzu spectrophotometer to analyse the absorbance spectra of the photocatalysts using $BaSO_4$ as reference in the wavelength range of λ = 200 - 800 nm.

PHOTOCATALYTIC ACTIVITY TESTS

The photocatalytic tests were performed in an aqueous solution utilizing MB dye as the model pollutant. An amount of 0.1 g of the prepared pure and Cu, Fe, and Ni-doped TiO_2 photocatalysts were mixed into 100 mL aqueous 2.5 mg/L MB solution to test the photocatalytic performance of each synthesised photocatalyst. The homemade box and a glass beaker of 250 mL in volume were used as the photoreactor for UV and visible light photocatalysis. For both the UV and visible light photocatalysis, two irradiation sources by an ultraviolet lamp with a wavelength peak at 365 nm and 90 W power, and a commercial halogen lamp PANASONIC with 25 W power were provided, respectively. For achieving the adsorption-desorption equilibrium before illumination by UV/Vis lamps, the solution was stirred in the dark using a magnetic stirrer for 1.5 h for each reaction. During the light irradiation, the reaction mixture was continuously stirred on a magnetic stirrer. The decolorization of dye was monitored using a UV–Vis spectrometer at λ_{max} = 664 nm. The decolorization percentage (D) was determined by (1), as given:

$$D(\%) = \frac{C_o - C}{C_o} \times 100\% \quad (1)$$

where C_o is initial concentrations of MB obtained before illumination and C is final concentrations at particular time (t), respectively. The photocatalytic tests were performed at room temperature and atmospheric pressure.

RESULTS AND DISCUSSION

X-RAY DIFFRACTION ANALYSIS

X-ray diffraction (XRD) was used to determine the phase, crystallinity, and structural properties of the photocatalysts. XRD analysis was conducted to clarify the presence of the initial bulk TiO_2 phases after calcination and the development of various crystalline TiO_2 phases induced by the various metal dopants mentioned previously. Figure 1 shows the wide-angle XRD patterns of pure TiO_2 and TiO_2 doped with 3, 6, and 9 mol% of each of Cu, Fe, and Ni metals. The XRD patterns of pure TiO_2 and Cu, Fe, and Ni-doped TiO_2 samples showed the dominant structure of anatase phase of the TiO_2 by the presence of crystalline peaks at 2θ of 25.3°, 37.9°, 48.0°, 53.9°, 55.0°, 62.8°, 68.8°, 70.2°, and 75.1°, reflecting the indices of (101), (004), (200), (105), (211), (204), (116), (220), and (215) tetragonal TiO_2 anatase phase planes, respectively (Krishnakumar et al. 2016). Peak related to precursors was not detected.

In general, the peaks for Cu-doped TiO_2, Fe-doped TiO_2, and Ni-doped TiO_2 samples almost matched those of pure TiO_2. No deviation of the peak position was observed with the changes in dopant concentration. This clearly indicates that dopant ions occupied the substitutional sites of Ti^{4+} without having distortion of the host lattice (Kavitha et al. 2016). The explanation for stabilizing TiO_2 in anatase process after doping with Ni at lower levels was due to the nearly identical Cu^{2+}, Fe^{3+}, and Ni^{2+} ionic radii (0.72, 0.69, and 0.72 Å, respectively) to that of Ti^{4+} (0.68 Å), which was found to replace some portion of Ti^{4+} ions in TiO_2 lattice (Ganesh et al. 2012; Sahoo & Gupta 2015). Furthermore, the formation of any

crystalline phase of Cu, Fe, and Ni species was not shown in XRD and the spectrum did not show any characteristic peak attributed to transition metal oxides. These results were similar with the findings obtained by Aguilar et al. (2013) and Sahoo and Gupta (2015).

The average crystallite size of all the synthesised pure and doped TiO_2 photocatalysts was obtained from the full width at half maximum (FWHM) of the most intense (101), (004), and (204) XRD peaks by using the following Scherrer equation:

$$d(nm) = \frac{0.9\lambda}{\beta \cos\theta} \quad (2)$$

where d is the average crystallite size; λ is the X-ray wavelength used in XRD analysis which is equal to 0.15406 nm; β is the full-width at half-maximum; and θ is the angle of diffraction for the broadening peak (Aguilar et al. 2013). Table 1 shows the average crystallite size of all the prepared samples. The XRD results obtained suggest that the size of the crystallite and the crystallization of the samples both decreased as the concentration of Cu, Fe, and Ni metal dopants in pure TiO_2 increased. The decrease in the size of crystallite with an increase in doping shows that Cu, Fe, and Ni doping inhibited TiO_2 crystallite growth. These findings conclude that copper, iron, and nickel affect the growth of crystallite during synthesis, showing that the above-mentioned metals have a great potential as doping agents (Aguilar et al. 2013; Nankya & Kim 2016).

NITROGEN PHYSISORPTION ANALYSIS

Nitrogen physisorption analysis was used to calculate the BET surface area of the photocatalysts. Table 1 summarizes the results obtained from the calculations. The addition of dopants to the host TiO_2 photocatalyst was observed to result in a larger surface area with the exception of 3 mol% Cu-doped TiO_2 sample. This was not in agreement with the fact that crystallite sizes decreased when the contents of Cu, Fe, and Ni increased. The reduction in crystallite size should lead to a greater specific surface area (Li et al. 2008; Vargas et al. 2015). The increase in the surface area of the doped samples could be due to the fact that metal ions supply additional nucleation sites during the precipitation and subsequent calcination steps. Unfortunately, it was not the case for 3 mol% Cu/TiO_2 as the total surface area was even lower (31.13 m^2/g) compared to that of pure TiO_2 (48.08 m^2/g). This might be due to the actual loading of Cu was so low in 3 mol% Cu-doped TiO_2 that Cu metal ions could not form nucleation centres in the skeletal structure of TiO_2 and could also be due to the pores blocked by copper species (Kerkez-kuyumcu et al. 2015).

FOURIER TRANSFORM INFRARED SPECTROSCOPY

The Fourier transform infrared (FTIR) spectroscopy provides evidence of the functional groups in TiO_2 photocatalysts. The FTIR spectra of pure and Cu, Fe, and Ni-doped TiO_2 photocatalysts are shown in Figure 2. The peaks at 3368, 3230, 3400, 3393, 3369, and 3214 cm^{-1} represent the existence of surface OH groups and H_2O molecules adsorbed on the surface and in the interlayer space (Kavitha et al. 2016). The peaks in between 2921 and 2853 cm^{-1} are assigned to C-H stretching vibrations of alkane groups. The alkane groups come from isopropanol and TTIP that are used in the synthesis process (Guo et al. 2007). The peaks at 1628, 1625, and 1621 cm^{-1} correspond to the stretching vibrations of OH groups, which are slowly decreasing with increasing the metal concentration in host TiO_2. The OH groups existing on the surface of TiO_2 enhance the photocatalytic performance of the photocatalysts due to OH groups serving as the main scavenger of the photogenerated charge carrier (Ali et al. 2017). Moreover, the wide absorption band from 500 to 1000 cm^{-1} corresponds to the vibration absorption of the Ti-O-Ti linkages in the TiO_2 molecules. The increase in metal concentrations could shift the Ti-O-Ti band to the lower wavenumbers and sharpening of the band and this is mainly because of the enhancement in crystallite size of the powders (Rajamannan et al. 2014a). In summary, the presence of strong functional groups at the interface of TiO_2 photocatalyst was showed from FTIR results in pure and TiO_2 doped photocatalysts. No peak for the precursors were observed in FTIR spectra.

FIELD EMISSION SCANNING ELECTRON MICROSCOPY

The morphology of the synthesised pure and doped TiO_2 photocatalysts was studied using Field Emission Scanning Electron Microscopy (FESEM) analysis. Figure 3 shows the FESEM images of pure and Cu, Fe, and Ni-doped TiO_2 photocatalysts. The pure TiO_2 powder shows irregular small granular clusters. By incorporating the dopant in the TiO_2 structure, the morphology and particle size of the photocatalyst change along with the increasing of Cu, Fe, and Ni concentrations. Figure 3 clearly shows the difference in size and morphology after doping with TiO_2. It is clearly observed that the doped TiO_2 photocatalysts depicted uniform distribution with irregular size spherical morphologies agglomeration which increased significantly with increasing amount of Ni ions in the host TiO_2 and the variability is finely tuned with increasing concentration of dopants (Sood et al. 2015). Moreover, the particle size was small as a result of calcination and the increase in agglomeration between metals and TiO_2 particles, which also indicates that metal doping can suppress the growth of TiO_2 particles. These

results are similar with the findings obtained by Nankya and Kim (2016) and Sakthivel and Jagannathan (2017). When metal ions doped into TiO_2 lattice, they preferred to stay in grain boundary regions or on the particle surface to inhibit TiO_2 crystal growth (Yang et al. 2015).

In addition, the elemental composition analysis of pure TiO_2 and Cu, Fe, and Ni-doped TiO_2 powders with 3, 6, and 9 mol% metal concentration in terms of mass% and atomic%, were performed using energy dispersive X-ray analysis (EDX) and the results are shown in Figure 4. The intense peaks in pure TiO_2 are associated with O (29.5%) and Ti (29.5%) elements. The measured mass% for Cu are around 1.9, 4.6 and 6.6% for 3, 6, and 9 mol% Cu/TiO_2, 1.9, 1.5, and 18.3% for Fe in 3, 6, and 9 mol% Fe/TiO_2, and 1.0, 0.9, and 1.6% for Ni in 3, 6, and 9 mol% Ni/TiO_2, respectively. The mass% and atomic% of the substances are tabulated in their respective images in Figure 4. The obtained results showed that presence of dopant is increased corresponding to loading of Cu, Fe, and Ni concentrations. Moreover, no residual acetate, chloride, nitrate, and other impurities presented in all samples.

UV-VIS DIFFUSE REFLECTANCE SPECTROSCOPY ANALYSIS

UV-Vis Diffuse Reflectance Spectroscopy (DRS) was performed to study the optical absorption characteristics of the prepared samples. The UV-Vis absorbance spectra of pure and Cu, Fe, and Ni-doped TiO_2 are shown in Figure 5. The TiO_2 photocatalyst showed an intense absorption in the UV region and as absorption edge of TiO_2 can be easily discerned. TiO_2 showed strong absorption between 200 and 390 nm, attributed to the photon energy of 3.24 eV, which is typical and identity of TiO_2. Upon Cu, Fe, and Ni doping, there was an enhancement of the optical absorption properties which gives a significant right shift in the absorption spectra towards longer wavelengths. The doped samples showed remarkable absorbance in the region of 400 - 800 nm, gradually demonstrating their strong visible light absorbance ability as compared to the pure TiO_2 (Singla et al. 2015). Furthermore, parallel increase in light absorbance with the increase in metal-doping concentration was also seen (Thu et al. 2016). Incorporation of Ni^{2+} ions into TiO_2 lattice shifted the fundamental absorption edge towards the longer wavelength. Since Ni-doped TiO_2 can absorb light in a wider range of wavelengths and utilize more light energy than pure TiO_2, a higher photocatalytic activity should be expected to Ni-doped TiO_2 photocatalysts. These results suggest that metal-doping certainly causing absorbance of visible light by TiO_2, enhancing light harvesting in both UV and visible light regions (Ganesh et al. 2012; Nankya & Kim 2016; Su et al. 2007).

The direct bandgap energies for all photocatalysts were estimated using (3) by extrapolating the linear region of the spectra to $\alpha = 0$ of a plot of $(\alpha hv)^2$ (Tauc plot) versus (hv) as shown in Figure 6.

$$(\alpha hv)^{1/n} = A(hv - E_g) \quad (3)$$

where E_g is the bandgap energy; h is Planck's constant; v is the frequency of vibration; hv is the photon energy; A is a proportional constant; α is the absorption coefficient; and n denotes the nature of the transition (Kerkez & Boz 2014). Depending on the nature of transition, n takes different values: For direct allowed transition $n = 1/2$, for indirect allowed transition $n = 2$, for direct forbidden transition $n = 3/2$, for indirect forbidden transition $n = 3$. Since the direct allowed transition is used in this experiment, $n = 1/2$ is used for the samples. The pure TiO_2 sample (Figure 5) shows absorption at around 383 nm (3.24 eV) (i.e. in the UV range) which occurred due to the charge transfer from the VB mainly formed by $2p$ orbitals of the oxide anions to the CB mainly formed by $3d$ t_{2g} orbitals of the Ti^{4+} cations (Venkatachalam et al. 2007). The estimated direct bandgap values of all samples shown in Table 2 are very close to the reported direct bandgap values for anatase. With the increase of Cu, Fe, and Ni concentrations, the bandgap energy of the TiO_2 photocatalyst increased systematically. This can be attributed to the introduction of new electron states in the band structure of TiO_2 upon Cu, Fe, and Ni doping (Hu et al. 2016; Manzoor et al. 2018). Any further increase in dopant concentration, the bandgap decreased. As can be observed from the trend, the bandgap value for 9 mol% Ni-doped TiO_2 is smaller (3.22 eV) than that of pure TiO_2. This trend is inconsistent with XRD results, where crystallite size initially decreased with doping and increased with an increasing amount of Cu, Fe, and Ni as well as TiO_2. The absorption edge wavelength of all prepared samples are shown in Table 2. At the same time on a higher level of doping (6 and 9 mol%) in addition to UV band, visible bands are also predicted. These bands are positioned at the range of 400 to 500 nm for 6 and 9 mol% doping amounts of Cu, Fe, and Ni metals (Rajamannan et al. 2014a, 2014b). However, in order to further enhance the photocatalytic activity, good interaction of Cu, Fe, and Ni with TiO_2 is required which could be confirmed by the FESEM images.

PHOTOCATALYTIC DECOLORIZATION OF METHYLENE BLUE

In this study, the photocatalytic activities of the prepared pure and Cu, Fe, and Ni-doped TiO_2 photocatalysts with different concentrations of metals were tested by the decolorization of MB under both UV and visible light

using homemade photoreactors. MB was selected because of its strong adsorption to metal oxide surfaces, well-defined optical absorption, and good resistance to light degradation (Jothibas et al. 2018). The photocatalytic experiments were carried out at an initial pH of 7.0 (Nakhate et al. 2010). The results of the photocatalytic decolorization of MB solution under UV and visible light irradiation in the presence of pure TiO_2 are shown in Figures 7 and 8, respectively. It is clear from the figure, with UV irradiation, pure TiO_2 photocatalyst exhibited higher photocatalytic activity than using visible light irradiation in decolorizing the MB solution. The photocatalytic decolorization of MB solution significantly increased with increasing the irradiation time. The pure TiO_2 photocatalyst displayed more than 98 and 97% decolorization rates for MB solution at the end of irradiation time of 5 h under UV and visible light, respectively. In a recent study, Zhang et al. (2015) studied the decolorization of MB solution using TiO_2 Degussa P25 and the process resulted in approximately 45% activity under visible light after 5 h of irradiation for the decolorization of MB. In another study by Kerkez-Kuyumcu et al. (2015), the pure TiO_2 prepared by a modified precipitation method showed a 44.18% decolorization rate for MB solution under visible light at the end of 5 h. Such results show that the pure TiO_2 prepared in this study using the sol-gel method has comparable levels of activity with the commercial TiO_2 Degussa P25 and TiO_2 prepared using a modified precipitation process. The difference in photocatalytic activity of pure TiO_2 under UV and visible light is very clear phenomenon, UV rays from the sunlight is less than 5% outdoor with little intensity (Inturi et al. 2014), the visible light employed for this study could be equate to sunlight, thus, the intensity of the UV content in the visible light is small.

In addition, as TiO_2 particles absorb the light corresponding to their bandgap energy, an electron is excited from the valence band (VB) to the TiO_2 conduction band (CB), creating a separation of the electron-hole charges as shown in (4) in the following:

$$TiO_2 + h\nu\ (\lambda < 390\,\text{nm}) \rightarrow e^- + h^+ \quad (4)$$

The charges can then react with the adsorbed oxygen and hydroxyl surface groups, creating reactive oxygen species that react with organic compounds resulting in the total decomposition of those compounds. The lifetime of electrons and holes must be long enough for any photocatalytic reaction to allow them to enter the photocatalyst's surface. Adding transition metal ions creates new trapping sites that influence the lifespan of the charge carriers. Once TiO_2 is doped with a transition metal, the photogenerated electrons in titanium are passed to the metal site CB, which serves as traps for the photogenerated electrons, increases the lifetime of the electron-hole pairs and increases the likelihood of reactions between the electron-hole pairs and the reactive oxygen species (Kerkez & Boz 2014). In this work, the visible light provided sufficient energy for the electrons to move from the VB to the CB and the Cu, Fe, and Ni dopants, served as an intermediate level of visible light electron excitation for MB decolorization purposes.

It is seen that the Cu-doped TiO_2 with Cu content of 3 mol% showed improved photocatalytic performance of 97.65 and 90% under UV and visible light shown in Figures 7(a) and 8(a), respectively. When the content of Cu doping reached to 6 and 9 mol%, the photocatalytic performance decreased to the lowest level of 89 and 81.4% under UV light and 62.4 and 55.7% under visible light at the end of irradiation time of 5 h, respectively, as compared to pure TiO_2 (Yang et al. 2015). The photocatalytic decolorization rate of MB as a function of time on 3, 6, and 9 mol% Fe-doped TiO_2 samples is given in Figures 7(b) and 8(b) under UV and visible light, respectively. It could be seen that the decolorization percentage is higher for pure TiO_2 under both UV and visible light rather than Fe-doped TiO_2 photocatalysts. The decolorization percentages were 96.86, 94.9, 92.38% for 3, 6, and 9 mol% Fe/TiO_2 under UV light, respectively. The Fe-doped TiO_2 samples had less photocatalytic efficiency than pure TiO_2 under visible light irradiation. The decolorization rate were 84.34, 60, and 62.42% at the end of 5 h visible light irradiation for 3, 6, and 9 mol% Fe-doped TiO_2 photocatalysts, respectively. This showed that the photocatalytic activity of the Fe-doped TiO_2 photocatalysts decreased with increasing the Fe concentration (Ali et al. 2017; Li et al. 2008).

The photocatalytic efficiency of Ni-doped TiO_2 samples is shown in Figures 7(c) and 8(c). It can be seen that among all Ni-doped TiO_2 photocatalysts, 3 mol% Ni/TiO_2 and 6 mol% Ni/TiO_2 showed the efficiency of 97.65 and 95.69% under UV light, respectively, which is close to that of pure TiO_2, 98%, and 9 mol% Ni/TiO_2 showed the lowest efficiency of 91.78%. The photodecolorization efficiency of 6 mol% Ni/TiO_2 powder showed the highest photocatalytic activity of 96.86% under visible light as compared to 3 and 9 mol% Ni/TiO_2, indicated that as the concentration of Ni further increased in TiO_2, the photocatalytic efficiency is gradually decreased (Ganesh et al. 2012). The photocatalytic efficiency of all prepared samples is given in Table 3.

Higher concentration of Cu and Fe (6 and 9 mol%) and Ni (9 mol%) in host TiO_2 favored the recombination of electron and hole and covered the active sites on the TiO_2 surface, thereby reducing the process. However, when the concentration of metal ion was higher than its optimal level, an excess amount of metal ion could not diffuse into the TiO_2 lattice, but deposited on the surface of TiO_2 particles. This led to the hindrance of UV light

penetration reaching the surface of TiO_2 which could block the active sites of TiO_2. Therefore, this mechanism inhibited the photocatalytic activity (Riaz et al. 2014). On the other hand, it was also reported that as the metal loading increases, agglomeration of metal particles is believed to occur and decrease the photocatalytic activity of the photocatalyst (Yoong et al. 2009). The development of the Schottky barrier in the metal-semiconductor contact region facilitated the separation of charge, thus, improved the photocatalytic efficiency in 3 mol% of Cu-doped TiO_2 photocatalyst. The formation of a new energy level in TiO_2 due to Cu-doped required the reduction of bandgap and increases the photocatalytic activity over pure TiO_2. Since the valence of Cu^{2+}, Fe^{3+}, and Ni^{2+} ions are less than that of Ti^{4+}, Cu, Fe, and Ni doping produces oxygen vacancies, which serve as the active sites for water dissociation on the metal-doped TiO_2 surfaces. It also catches the holes to limit the recombination of electron-hole pairs and to donate in oxidation of organic pollutants (Yang et al. 2015; Zhang et al. 2015).

Doping TiO_2 with Ni introduces a new energy level (Ni impurity level) by the dispersion of metal particles in the TiO_2 matrix which acts as an electron trap (Ni et al. 2007). The electron trap will prevent the recombination of electron-hole pairs during the irradiation, thus, increasing the lifetime of charge carriers. Ni-doped TiO_2 not only boosts the separation efficiency of photoinduced electrons and holes, but also increases the visible light absorption due to bandgap shifting (Haque et al. 2013). It is well known that in heterogeneous photocatalysis process, the hydroxyl radicals (•OH) are a primary oxidant. When the TiO_2 particle absorbs photon energy of equal to or greater than its bandgap, an electron may be promoted from the VB to the CB leaving behind an electron vacancy or 'hole' in the VB. Likewise, an electron can be transferred from impurity level to TiO_2 CB through the absorption of photon energy equal to or greater than its bandgap. The vacancy created in the impurity band acts as an electron trap. The electron generated in VB of TiO_2 is trapped by the electron trap which reduces the recombination of the electron-hole pairs. If charge separation is maintained, the electron and hole may migrate to the catalyst surface where they participate in redox reactions with sorbed species. Hole (h^+) may react with surface-bound H_2O or OH^- to produce the •OH and the electrons (e^-) present at the CB are scavenged or picked up by Cu^{2+}, Fe^{3+}, and Ni^{2+} ions, which then transfer them to the oxygen molecules to form the strong oxidative superoxide radical anion (Haque et al. 2013). These reactive species play an important role in the decolorization of MB (Ali et al. 2017). The increase in photocatalytic activity by increasing Ni dopant concentration from 3 to 6 mol% under visible light may be due to the shifting of the bandgap absorption edge to the visible light region, absorbing the light of longer wavelength. Another explanation for this could be attributed to the fact that Ni-doped TiO_2 introduces new trapping sites which affect the lifetime of charge carriers by splitting the time of arrival of photogenerated electrons and holes to reach the photocatalyst surface and, thus, reduce the recombination of electron-hole (Haque et al. 2013).

TABLE 1. Average crystallite size and BET surface area of the prepared photocatalysts

Photocatalysts	d (nm)	Total surface area (m^2/g)
Pure TiO_2	13.42	42.08
3 mol% Cu/TiO_2	12.75	31.13
6 mol% Cu/TiO_2	11.77	53.09
9 mol% Cu/TiO_2	12.12	58.83
3 mol% Fe/TiO_2	8.52	53.34
6 mol% Fe/TiO_2	5.91	100.21
9 mol% Fe/TiO_2	5.70	84.50
3 mol% Ni/TiO_2	8.27	73.18
6 mol% Ni/TiO_2	8.28	74.12
9 mol% Ni/TiO_2	7.03	111.30

TABLE 2. Optical properties of pure and Cu, Fe, and Ni-doped TiO_2 photocatalysts

Photocatalysts	Bandgap energy (eV)	Absorption edge wavelength (nm)
Pure TiO_2	3.24	383
3 mol% Cu/TiO_2	3.42	363
6 mol% Cu/TiO_2	3.38	367
9 mol% Cu/TiO_2	3.26	380
3 mol% Fe/TiO_2	3.37	368
6 mol% Fe/TiO_2	3.38	367
9 mol% Fe/TiO_2	3.29	377
3 mol% Ni/TiO_2	3.35	370
6 mol% Ni/TiO_2	3.35	370
9 mol% Ni/TiO_2	3.22	385

TABLE 3. Decolorization percentage of MB dye under both UV and visible light irradiation

Photocatalysts	Efficiency (%)/UV light	Efficiency (%)/visible light
Pure TiO_2	98	97.26
3 mol% Cu/TiO_2	97.65	90
6 mol% Cu/TiO_2	89	55.77
9 mol% Cu/TiO_2	81.4	64.77
3 mol% Fe/TiO_2	96.86	84.34
6 mol% Fe/TiO_2	94.9	60
9 mol% Fe/TiO_2	82.38	62.42
3 mol% Ni/TiO_2	97.65	94.32
6 mol% Ni/TiO_2	95.69	96.86
9 mol% Ni/TiO_2	91.78	76.90

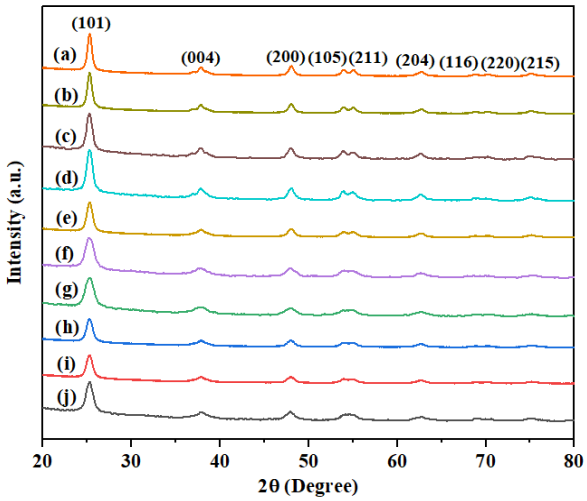

FIGURE 1. X-ray diffraction patterns of (a) pure TiO_2, (b) 3 mol% Cu/TiO_2, (c) 6 mol% Cu/TiO_2, (d) 9 mol% Cu/TiO_2, (e) 3 mol% Fe/TiO_2, (f) 6 mol% Fe/TiO_2, (g) 9 mol% Fe/TiO_2, (h) 3 mol% Ni/TiO_2, (i) 6 mol% Ni/TiO_2, and (j) 9 mol% Ni/TiO_2 photocatalysts

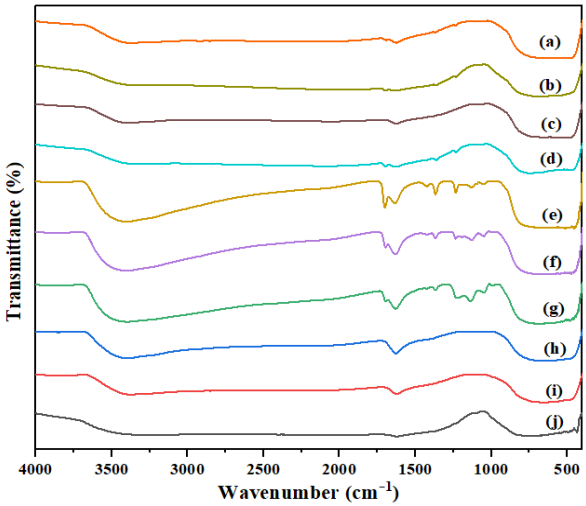

FIGURE 2. FTIR spectra of (a) pure TiO_2, (b) 3 mol% Cu/TiO_2, (c) 6 mol% Cu/TiO_2, (d) 9 mol% Cu/TiO_2, (e) 3 mol% Fe/TiO_2, (f) 6 mol% Fe/TiO_2, (g) 9 mol% Fe/TiO_2, (h) 3 mol% Ni/TiO_2, (i) 6 mol% Ni/TiO_2, and (j) 9 mol% Ni/TiO_2 photocatalysts

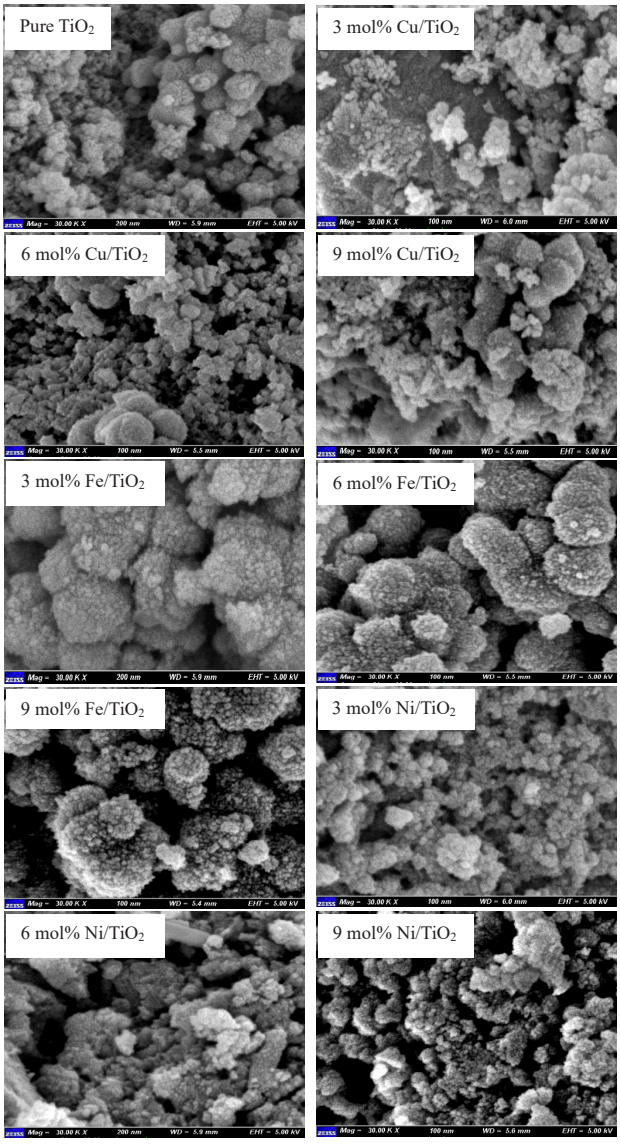

FIGURE 3. FESEM micrographs of pure TiO_2 and Cu, Fe, and Ni-doped TiO_2 photocatalysts with different concentration of transition metals

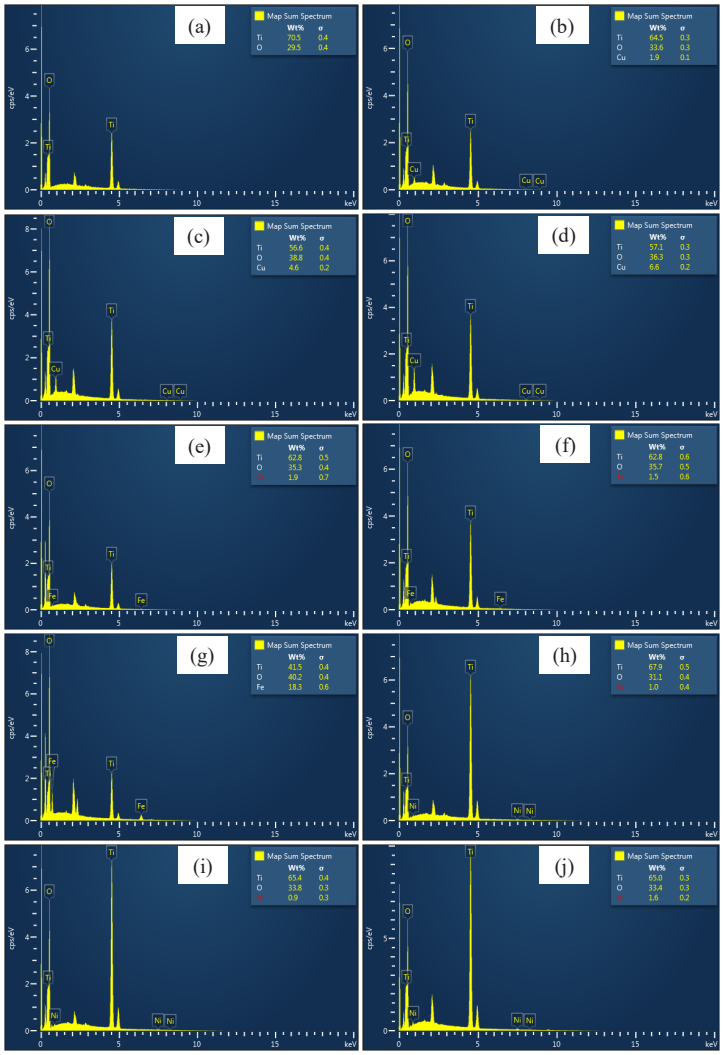

FIGURE 4. FEDX spectra of (a) pure TiO_2, (b) 3 mol% Cu/TiO_2, (c) 6 mol% Cu/TiO_2, (d) 9 mol% Cu/TiO_2, (e) 3 mol% Fe/TiO_2, (f) 6 mol% Fe/TiO_2, (g) 9 mol% Fe/TiO_2, (h) 3 mol% Ni/TiO_2, (i) 6 mol% Ni/TiO_2, and (j) 9 mol% Ni/TiO_2 photocatalysts

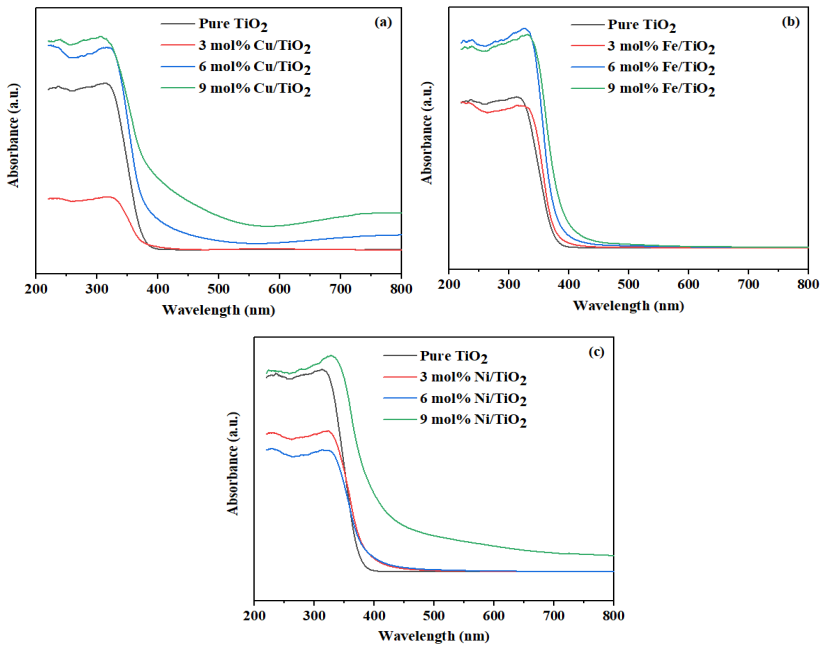

FIGURE 5. UV-Vis absorption spectra of (a) Cu-doped TiO_2, (b) Fe-doped TiO_2, and (c) Ni-doped TiO_2 photocatalysts with different concentration of metals and pure TiO_2 is also used as reference in all cases for comparison with the results obtained

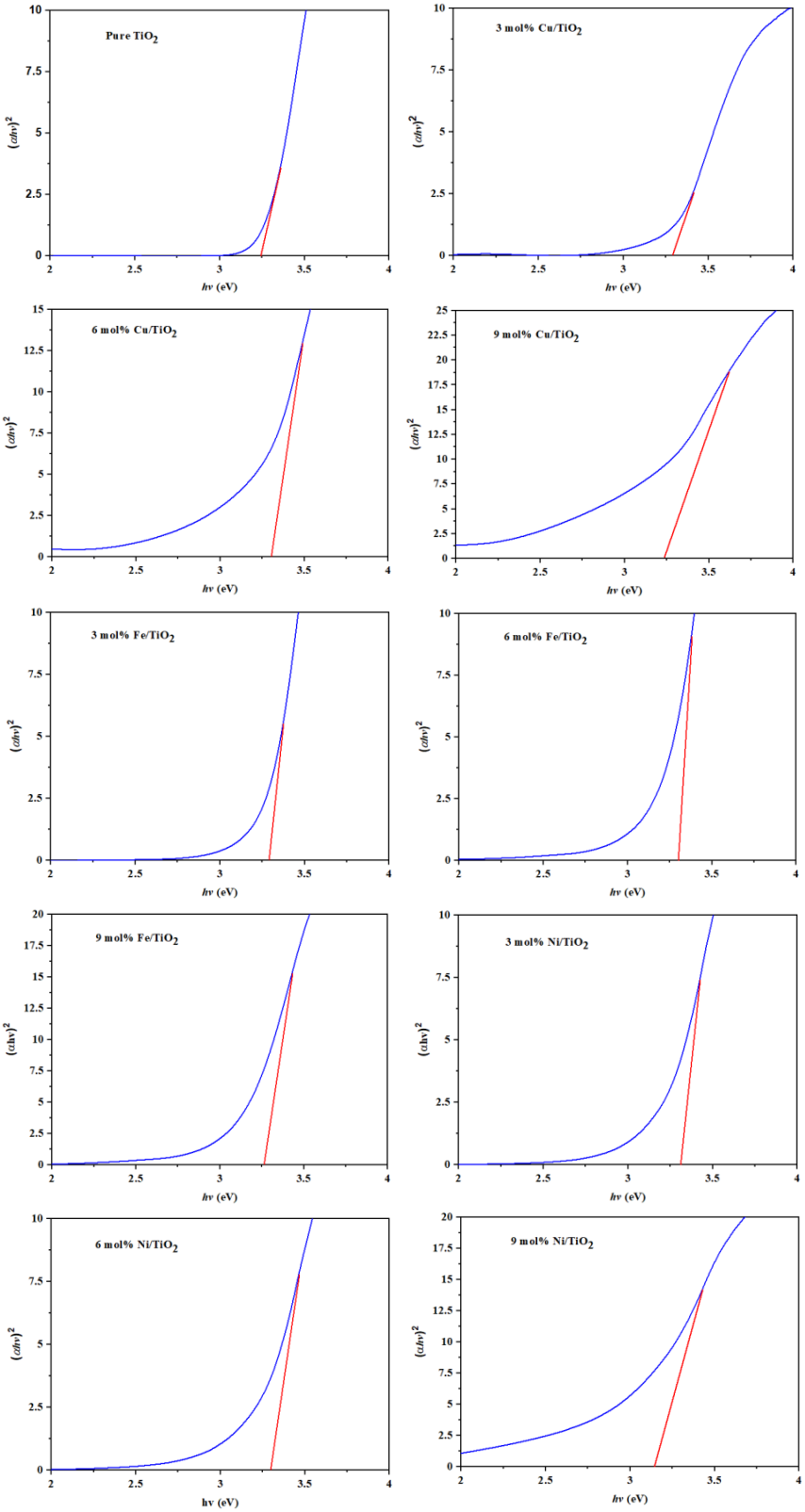

FIGURE 6. Plots of $(\alpha h\nu)^2$ versus $h\nu$ (Tauc plot) for the estimation of the bandgap energy

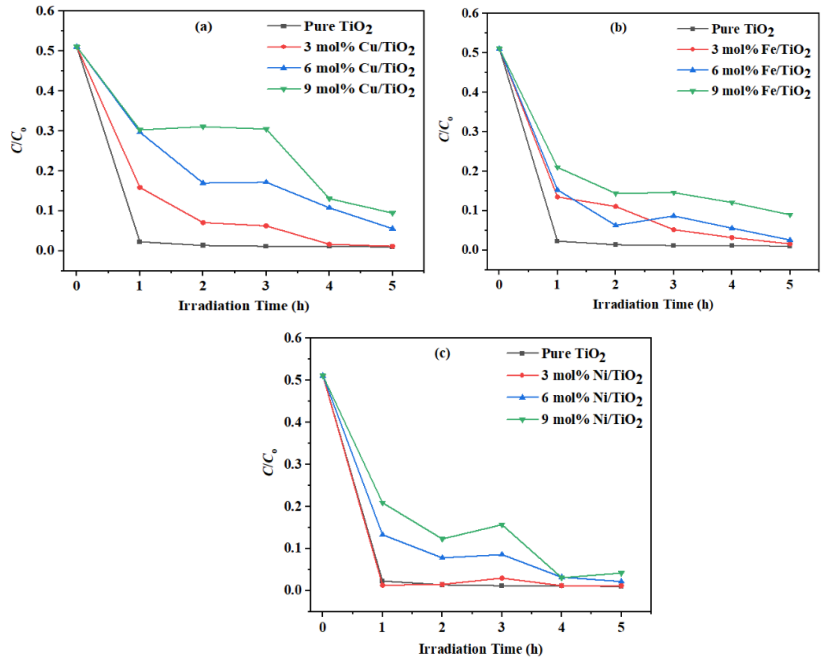

FIGURE 7. The photocatalytic decolorization of MB under UV light irradiation using pure TiO_2 and (a) Cu/TiO_2, (b) Fe/TiO_2, and Ni/TiO_2 photocatalysts with different metal concentrations

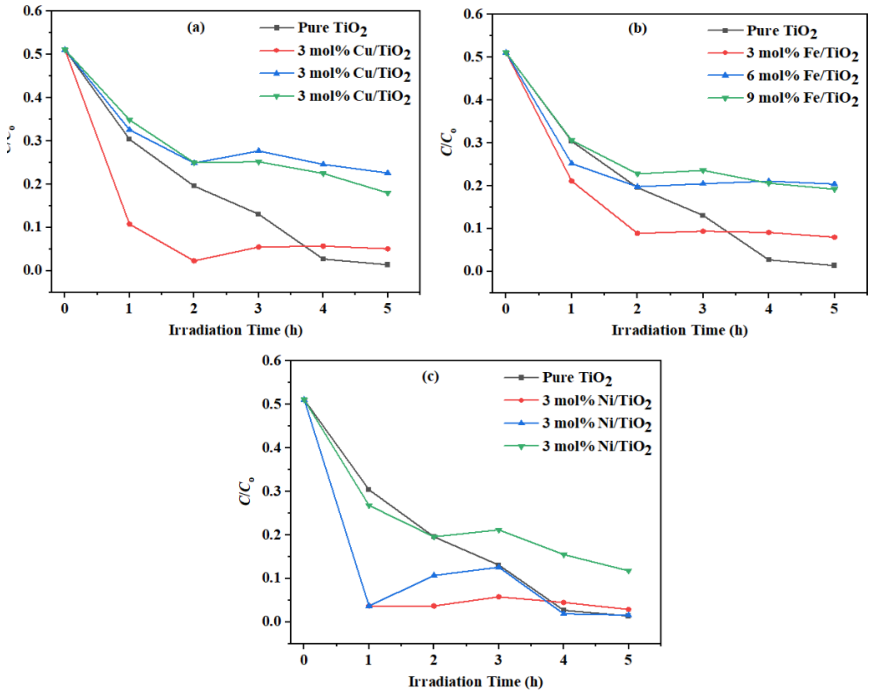

FIGURE 8. The photocatalytic decolorization of MB under visible light irradiation using pure TiO_2 and (a) Cu/TiO_2, (b) Fe/TiO_2, and Ni/TiO_2 photocatalysts with different metal concentrations

Conclusion

In this work, the pure and Cu, Fe, and Ni-doped TiO_2 photocatalysts, were successfully prepared using the sol-gel method. The XRD patterns of all pure TiO_2 and Cu/TiO_2, Fe/TiO_2, and Ni/TiO_2 samples showed the anatase phase structure of TiO_2 predominantly and the average crystallite size of the base TiO_2 was decreased after doping with transition metals. The presence of strong functional groups on the surface and at the interface of TiO_2 particles was showed by FTIR. The FESEM analysis indicated that the particle size of the prepared doped samples was uniform with spherical morphology and their variability was finely tuned with increasing dopant concentration, while EDX results showed that TiO_2 was successfully incorporated Cu, Fe, and Ni metals onto its surface. The BET analysis showed that the specific surface area of pure TiO_2 was 42.08 m^2/g and the surface area of the doped photocatalysts increased with the increasing amount of dopant to 111.3 m^2/g for 9 mol% Ni-doped TiO_2 and the pore size of the photocatalysts was confirmed to be in mesoporous region by the BJH method. The optical properties of all samples were carried out using UV-DRS measurements and their obtained bandgap energies were in the range of 3.22 - 3.42 eV. The pure TiO_2 photocatalyst displayed more than 98% and 97% decolorization rates for MB solution at the end of irradiation time of 5 h under UV and visible light, respectively. Among all the doped photocatalysts, 3 mol% Ni/TiO_2 showed the highest decolorization efficiency of 97.6% under UV light and 6 mol% Ni/TiO_2 photocatalysts showed efficiency of 96.86% under visible light irradiation in decolorizing MB dye.

Acknowledgements

This work is supported by the UTM Research University Grant via UTM Transdisciplinary Research Grant Scheme (Vot No. 07G30) and Kabul University, Afghanistan for postgraduate scholarship (Jawed Qaderi).

References

Adekoya, D., Tahir, M. & Amin, N.A.S. 2019. Recent trends in photocatalytic materials for reduction of carbon dioxide to methanol. *Renewable and Sustainable Energy Reviews* 116: 109389.

Aguilar, T., Navas, J., Alcántara, R., Fernández-Lorenzo, C., Gallardo, J.J., Blanco, G. & Martín-Calleja, J. 2013. A route for the synthesis of Cu-doped TiO_2 nanoparticles with a very low bandgap. *Chemical Physics Letters* 571: 49-53.

Ahmad, A.L. & Puasa, S.W. 2007. Reactive dyes decolourization from an aqueous solution by combined coagulation/micellar-enhanced ultrafiltration process. *Chemical Engineering Journal* 132(1-3): 257-265.

Ali, T., Tripathi, P., Azam, A., Raza, W., Ahmed, A.S., Ahmed, A. & Muneer, M. 2017. Photocatalytic performance of Fe-doped TiO_2 nanoparticles under visible-light irradiation. *Materials Research Express* 4(1): 015022.

Derudi, M., Venturini, G., Lombardi, G., Nano, G. & Rota, R. 2007. Biodegradation combined with ozone for the remediation of contaminated soils. *European Journal of Soil Biology* 43(5-6): 297-303.

Edelmannová, M., Lin, K.Y., Wu, J.C., Troppová, I., Čapek, L. & Kočí, K. 2018. Photocatalytic hydrogenation and reduction of CO_2 over CuO/TiO_2 photocatalysts. *Applied Surface Science* 454: 313-318.

Ganesh, I., Gupta, A.K., Kumar, P.P., Sekhar, P.S.C., Radha, K., Padmanabham, G. & Sundararajan, G. 2012. Preparation and characterization of Ni-doped materials for photocurrent and photocatalytic applications. *The Scientific World Journal* 2012: 1-16.

Guo, G., He, C., Wang, Z., Gu, F. & Han, D. 2007. Synthesis of titania and titanate nanomaterials and their application in environmental analytical chemistry. *Talanta* 72(5): 1687-1692.

Haque, M.M., Khan, A., Umar, K., Mir, N.A., Muneer, M., Harada, T. & Matsumura, M. 2013. Synthesis, characterization and photocatalytic activity of visible light induced Ni-doped TiO_2. *Energy and Environment Focus* 2(1): 73-78.

Hu, J., Zhan, L., Zhang, G., Zhang, Q., Du, L., Tung, C.H. & Wang, Y. 2016. Effects of substitutional dopants on the photoresponse of a polyoxotitanate cluster. *Inorganic Chemistry* 55(17): 8493-8501.

Inturi, S.N.R., Boningari, T., Suidan, M. & Smirniotis, P.G. 2014. Visible-light-induced photodegradation of gas phase acetonitrile using aerosol-made transition metal (V, Cr, Fe, Co, Mn, Mo, Ni, Cu, Y, Ce, and Zr) doped TiO_2. *Applied Catalysis B: Environmental* 144: 333-342.

Jothibas, M., Manoharan, C., Jeyakumar, S.J., Praveen, P., Punithavathy, I.K. & Richard, J.P. 2018. Synthesis and enhanced photocatalytic property of Ni doped ZnS nanoparticles. *Solar Energy* 159: 434-443.

Kavitha, V., Ramesh, P.S. & Geetha, D. 2016. Synthesis of Cu loaded TiO_2 nanoparticles for the improved photocatalytic degradation of rhodamine B. *International Journal of Nanoscience* 15(5-6): 1660002.

Kerkez, Ö. & Boz, İ. 2014. Photo (electro) catalytic activity of Cu^{2+}-modified TiO_2 nanorod array thin films under visible light irradiation. *Journal of Physics and Chemistry of Solids* 75(5): 611-618.

Kerkez-Kuyumcu, Ö., Kibar, E., Dayıoğlu, K., Gedik, F., Akın, A.N. & Özkara-Aydınoğlu, Ş. 2015. A comparative study for removal of different dyes over M/TiO_2 (M = Cu, Ni, Co, Fe, Mn and Cr) photocatalysts under visible light irradiation. *Journal of Photochemistry and Photobiology A: Chemistry* 311: 176-185.

Krishnakumar, V., Boobas, S., Jayaprakash, J., Rajaboopathi, M., Han, B. & Louhi-Kultanen, M. 2016. Effect of Cu doping on TiO_2 nanoparticles and its photocatalytic activity under visible light. *Journal of Materials Science: Materials in Electronics* 27(7): 7438-7447.

Li, Z., Shen, W., He, W. & Zu, X. 2008. Effect of Fe-doped TiO_2 nanoparticle derived from modified hydrothermal process on the photocatalytic degradation performance on methylene blue. *Journal of Hazardous Materials* 155(3): 590-594.

Liu, S.X., Chen, X.Y. & Chen, X. 2007. A TiO_2/AC composite photocatalyst with high activity and easy separation prepared by a hydrothermal method. *Journal of Hazardous Materials* 143(1-2): 257-263.

Manzoor, M., Rafiq, A., Ikram, M., Nafees, M. & Ali, S. 2018. Structural, optical, and magnetic study of Ni-doped TiO_2 nanoparticles synthesized by sol-gel method. *International Nano Letters* 8(1): 1-8.

Mo, J.H., Lee, Y.H., Kim, J., Jeong, J.Y. & Jegal, J. 2008. Treatment of dye aqueous solutions using nanofiltration polyamide composite membranes for the dye wastewater reuse. *Dyes and Pigments* 76(2): 429-434.

Nakhate, G.G., Nikam, V.S., Kanade, K.G., Arbuj, S., Kale, B.B. & Baeg, J.O. 2010. Hydrothermally derived nanosized Ni-doped TiO_2: A visible light driven photocatalyst for methylene blue degradation. *Materials Chemistry and Physics* 124(2-3): 976-981.

Nankya, R. & Kim, K.N. 2016. Sol-gel synthesis and characterization of Cu-TiO_2 nanoparticles with enhanced optical and photocatalytic properties. *Journal of Nanoscience and Nanotechnology* 16(11): 11631-11634.

Thu, T.N.T., Thi, N.N., Quang, V.T., Hong, K.N., Minh, N.T. & Hoai, N.L.T. 2016. Synthesis, characterisation, and effect of pH on degradation of dyes on copper-doped TiO_2. *Journal of Experimental Nanoscience* 11(3): 226-238.

Ni, M., Leung, M.K., Leung, D.Y. & Sumathy, K. 2007. A review and recent developments in photocatalytic water-splitting using TiO_2 for hydrogen production. *Renewable and Sustainable Energy Reviews* 11(3): 401-425.

Rajamannan, B., Mugundan, S., Viruthagiri, G., Praveen, P. & Shanmugam, N. 2014a. Linear and nonlinear optical studies of bare and copper doped TiO_2 nanoparticles via sol gel technique. *Spectrochimica Acta Part A: Molecular and Biomolecular Spectroscopy* 118: 651-656.

Rajamannan, B., Mugundan, S., Viruthagiri, G., Shanmugam, N., Gobi, R. & Praveen, P. 2014b. Preparation, structural and morphological studies of Ni doped titania nanoparticles. *Spectrochimica Acta Part A: Molecular and Biomolecular Spectroscopy* 128: 218-224.

Rauf, M.A. & Ashraf, S.S. 2009. Fundamental principles and application of heterogeneous photocatalytic degradation of dyes in solution. *Chemical Engineering Journal* 151(1-3): 10-18.

Riaz, N., Kait, C.F., Man, Z., Dutta, B.K., Ramli, R.M. & Khan, M.S. 2014. Visible light photodegradation of azo dye by Cu/TiO_2. *Advanced Materials Research* 917: 151-159.

Sahoo, C. & Gupta, A.K. 2015. Characterization and photocatalytic performance evaluation of various metal ion-doped microstructured TiO_2 under UV and visible light. *Journal of Environmental Science and Health, Part A* 50(7): 659-668.

Sakthivel, T. & Jagannathan, K. 2017. Structural, optical, morphological and elemental analysis on sol-gel synthesis of Ni doped TiO_2 nanocrystallites. *Mechanics, Materials Science & Engineering Journal* 9(1): 2412-5954.

Salehi, M., Hashemipour, H. & Mirzaee, M. 2012. Experimental study of influencing factors and kinetics in catalytic removal of methylene blue with TiO_2 nanopowder. *American Journal of Environmental Engineering* 2(1): 1-7.

Shehzad, N., Tahir, M., Johari, K., Murugesan, T. & Hussain, M. 2018. A critical review on TiO_2 based photocatalytic CO_2 reduction system: Strategies to improve efficiency. *Journal of CO_2 Utilization* 26: 98-122.

Singla, P., Pandey, O.P. & Singh, K. 2015. Study of photocatalytic degradation of environmentally harmful phthalate esters using Ni-doped TiO_2 nanoparticles. *International Journal of Environmental Science and Technology* 13(3): 849-856.

Sood, S., Umar, A., Mehta, S.K. & Kansal, S.K. 2015. Highly effective Fe-doped TiO_2 nanoparticles photocatalysts for visible-light driven photocatalytic degradation of toxic organic compounds. *Journal of Colloid and Interface Science* 450: 213-223.

Soutsas, K., Karayannis, V., Poulios, I., Riga, A., Ntampegliotis, K., Spiliotis, X. & Papapolymerou, G. 2010. Decolorization and degradation of reactive azo dyes via heterogeneous photocatalytic processes. *Desalination* 250(1): 345-350.

Su, B., Wang, K., Bai, J., Mu, H., Tong, Y., Min, S., She, S. & Lei, Z. 2007. Photocatalytic degradation of methylene blue on Fe^{3+}-doped TiO_2 nanoparticles under visible light irradiation. *Frontiers of Chemistry in China* 2(4): 364-368.

Vargas, D.X.M., De la Rosa, J.R., Lucio-Ortiz, C.J., Hernández-Ramirez, A., Flores-Escamilla, G.A. & Garcia, C.D. 2015. Photocatalytic degradation of trichloroethylene in a continuous annular reactor using Cu-doped TiO_2 catalysts by sol-gel synthesis. *Applied Catalysis B: Environmental* 179: 249-261.

Venkatachalam, N., Palanichamy, M. & Murugesan, V. 2007. Sol-gel preparation and characterization of nanosize TiO_2: Its photocatalytic performance. *Materials Chemistry and Physics* 104(2-3): 454-459.

Yang, X.J., Shu, W., Sun, H.M., Wang, X.B. & Lian, J.S. 2015. Preparation and photocatalytic performance of Cu-doped TiO_2 nanoparticles. *Transactions of Nonferrous Metals Society of China* 25(2): 504-509.

Yoong, L.S., Chong, F.K. & Dutta, B.K. 2009. Development of copper-doped TiO_2 photocatalyst for hydrogen production under visible light. *Energy* 34(10): 1652-1661.

Zhang, F., Cheng, Z., Kang, L., Cui, L., Liu, W., Xu, X., Hou, G. & Yang, H. 2015. A novel preparation of Ag-doped TiO_2 nanofibers with enhanced stability of photocatalytic activity. *RSC Advances* 5(41): 32088-32091.

Jawed Qaderi & Che Rozid Mamat*
Department of Chemistry
Faculty of Science
Universiti Teknologi Malaysia
81310 UTM Johor Bahru, Johor Darul Takzim
Malaysia

Jawed Qaderi
Department of Physical Chemistry
Faculty of Chemistry
Kabul University
Jamal Mina, Kabul
Afghanistan

Aishah Abdul Jalil
School of Chemical and Energy Engineering
Faculty of Engineering
Universiti Teknologi Malaysia
81310 UTM Johor Bahru, Johor Darul Takzim
Malaysia

Aishah Abdul Jalil
Centre of Hydrogen Energy
Institute of Future Energy
Universiti Teknologi Malaysia
81310 UTM Johor Bahru, Johor Darul Takzim
Malaysia

*Corresponding author; email: cherozid@tm.my

Received: 7 April 2020
Accepted: 23 June 2020